Atmospheric Environment 164 (2017) 325–336

Contents lists available at ScienceDirect

Atmospheric Environment

journal homepage: www.elsevier.com/locate/atmosenv

Impact of evolving isoprene mechanisms on simulated formaldehyde: An inter-comparison supported by *in situ* observations from SENEX

Margaret R. Marvin [a, *], Glenn M. Wolfe [b, c], Ross J. Salawitch [a, d, e], Timothy P. Canty [d], Sandra J. Roberts [a], Katherine R. Travis [f, g], Kenneth C. Aikin [h, i], Joost A. de Gouw [h, i], Martin Graus [h, i, 1], Thomas F. Hanisco [c], John S. Holloway [h, i], Gerhard Hübler [h, i], Jennifer Kaiser [f], Frank N. Keutsch [f, j], Jeff Peischl [h, i], Ilana B. Pollack [k], James M. Roberts [i], Thomas B. Ryerson [i], Patrick R. Veres [h, i], Carsten Warneke [h, i]

[a] Department of Chemistry and Biochemistry, University of Maryland College Park, College Park, MD 20742, USA
[b] Joint Center for Earth Systems Technology, University of Maryland Baltimore County, Baltimore, MD 21250, USA
[c] Atmospheric Chemistry and Dynamics Laboratory, NASA Goddard Space Flight Center, Greenbelt, MD 20771, USA
[d] Department of Atmospheric and Oceanic Science, University of Maryland College Park, College Park, MD 20742, USA
[e] Earth System Science Interdisciplinary Center, University of Maryland College Park, College Park, MD 20742, USA
[f] School of Engineering and Applied Sciences, Harvard University, Cambridge, MA 02138, USA
[g] Department of Earth and Planetary Sciences, Harvard University, Cambridge, MA 02138, USA
[h] Cooperative Institute for Research in Environmental Sciences, University of Colorado Boulder, Boulder, CO 80309, USA
[i] Chemical Sciences Division, NOAA Earth System Research Laboratory, Boulder, CO 80305, USA
[j] Department of Chemistry and Chemical Biology, Harvard University, Cambridge, MA 02138, USA
[k] Department of Atmospheric Science, Colorado State University, Fort Collins, CO 80523, USA

HIGHLIGHTS

- All considered mechanisms underestimate observed HCHO by at least 15%.
- Mechanistic differences are driven by second- and late-generation isoprene oxidation.
- Recommendations are provided for CB6r2 and incorporated into new mechanism CB6r2-UMD.
- Simulated HCHO impacts modeled ozone production rates.

ARTICLE INFO

Article history:
Received 4 March 2017
Received in revised form
26 May 2017
Accepted 29 May 2017
Available online 30 May 2017

Keywords:
Formaldehyde
Isoprene
Gas-phase chemical mechanisms
Box model
SENEX
Air quality

ABSTRACT

Isoprene oxidation schemes vary greatly among gas-phase chemical mechanisms, with potentially significant ramifications for air quality modeling and interpretation of satellite observations in biogenic-rich regions. In this study, *in situ* observations from the 2013 SENEX mission are combined with a constrained 0-D photochemical box model to evaluate isoprene chemistry among five commonly used gas-phase chemical mechanisms: CB05, CB6r2, MCMv3.2, MCMv3.3.1, and a recent version of GEOS-Chem. Mechanisms are evaluated and inter-compared with respect to formaldehyde (HCHO), a high-yield product of isoprene oxidation. Though underestimated by all considered mechanisms, observed HCHO mixing ratios are best reproduced by MCMv3.3.1 (normalized mean bias = −15%), followed by GEOS-Chem (−17%), MCMv3.2 (−25%), CB6r2 (−32%) and CB05 (−33%). Inter-comparison of HCHO production rates reveals that major restructuring of the isoprene oxidation scheme in the Carbon Bond mechanism increases HCHO production by only ~5% in CB6r2 relative to CB05, while further refinement of the complex isoprene scheme in the Master Chemical Mechanism increases HCHO production by ~16% in MCMv3.3.1 relative to MCMv3.2. The GEOS-Chem mechanism provides a good approximation of the explicit isoprene chemistry in MCMv3.3.1 and generally reproduces the magnitude and source distribution of HCHO production rates. We analytically derive improvements to the isoprene scheme in CB6r2 and incorporate these changes into a new mechanism called CB6r2-UMD, which is designed to preserve computational efficiency. The CB6r2-UMD mechanism mimics production of HCHO in MCMv3.3.1 and demonstrates

* Corresponding author.
E-mail address: mmarvin@umd.edu (M.R. Marvin).
[1] Now at: Institute of Atmospheric and Cryospheric Sciences, University of Innsbruck, Innsbruck, Austria.

http://dx.doi.org/10.1016/j.atmosenv.2017.05.049

good agreement with observed mixing ratios from SENEX (−14%). Improved simulation of HCHO also impacts modeled ozone: at ~0.3 ppb NO, the ozone production rate increases ~3% between CB6r2 and CB6r2-UMD, and rises another ~4% when HCHO is constrained to match observations.

1. Introduction

Isoprene (C_5H_8) is a reactive biogenic hydrocarbon that fuels oxidative chemistry in many terrestrial regions. Annual isoprene emissions are ~500 Tg yr^{-1}, accounting for nearly one-third of global non-methane volatile organic compound (VOC) emissions (Guenther et al., 2012). Once emitted, isoprene is quickly oxidized by atmospheric OH, which limits the isoprene lifetime to <1–3 hr. The oxidation of isoprene by OH generates many products, including formaldehyde (HCHO), methyl vinyl ketone (MVK), methacrolein (MACR), and numerous other oxygenated organic compounds. Depending on conditions for NO_x ($NO_x = NO + NO_2$), the oxidation of isoprene can also produce ozone (Trainer et al., 1987) or secondary organic aerosol (SOA) (Jacobs et al., 2014; Kroll et al., 2006; Lin et al., 2013; Paulot et al., 2009b; Surratt et al., 2010; Surratt et al., 2006), both of which are hazardous to human health (EPA, 2009, 2013) and are strong climate forcers (IPCC, 2013).

The oxidation of isoprene by OH leads to the formation of isoprene hydroxy peroxy radicals ($ISOPO_2$), with subsequent chemistry determined by NO_x conditions. In the presence of NO_x, $ISOPO_2$ reacts with NO to form MVK, MACR, and HCHO (Paulson and Seinfeld, 1992). In a minor channel, the reaction of $ISOPO_2$ with NO produces organic nitrates (ISOPN), which undergo oxidation by OH to form small nitrated organic products (Paulot et al., 2009a). The high-NO_x reaction pathways of $ISOPO_2$ result in the net conversion of NO to NO_2, which promotes production of tropospheric ozone. Under low-NO_x conditions, $ISOPO_2$ may react with HO_2 or RO_2 or isomerize. Reaction with HO_2 produces isoprene hydroxy hydroperoxides (ISOPOOH), which undergo oxidation by OH to form isoprene epoxydiols (IEPOX), known precursors of SOA (Paulot et al., 2009b). Reaction of $ISOPO_2$ with RO_2 mainly produces MVK, MACR, and HCHO (Saunders et al., 2003). Isomerization of $ISOPO_2$ proceeds by intramolecular hydrogen transfer, specifically via either 1,5-H or 1,6-H shift (Da Silva et al., 2010; Peeters et al., 2009). The 1,5-H shift forms an unstable intermediate that degrades into MVK, MACR, and HCHO. The 1,6-H shift produces hydroperoxyenals (HPALD), which photolyze to form small VOCs and regenerate OH (Crounse et al., 2011; Peeters and Müller, 2010; Peeters et al., 2014; Wolfe et al., 2012).

Representations of isoprene chemistry in gas-phase chemical mechanisms can vary widely (Table 1). Inconsistencies arise from differences in complexity, choice of kinetic rate constants, and incorporation of results from recent literature. Previous mechanism inter-comparison studies have shown that different interpretations of atmospheric chemistry lead to conflicting representations of species important to air quality and climate, including ozone (Coates and Butler, 2015; Emmerson and Evans, 2009; Knote et al., 2015; Saylor and Stein, 2012; Yu et al., 2010). Although some mechanism inter-comparisons have focused on isoprene oxidation in the past (Archibald et al., 2010; Fan and Zhang, 2004; Pöschl et al., 2000; Squire et al., 2015; von Kuhlmann et al., 2004; Zhang et al., 2011), the scientific understanding of isoprene chemistry has evolved rapidly in recent years, with discoveries such as epoxide formation (Paulot et al., 2009b), peroxy radical isomerization (Peeters et al., 2009), and OH regeneration (Paulot et al., 2009b; Peeters et al., 2009; Wolfe et al., 2012). Furthermore, the limited availability of *in situ* observations has restricted our ability to quantitatively evaluate mechanisms against ground truth.

Formaldehyde is produced in high yield throughout the isoprene cascade (Tuazon and Atkinson, 1990). The chemical link between HCHO and isoprene also depends on NO_x, which determines the chemical fate of $ISOPO_2$ and subsequent yield of organic products (Wolfe et al., 2016a). Although complex, the relationships between these species are crucial to many modeling applications. In air quality simulations, for example, the production of HCHO from VOCs such as isoprene is indicative of the effects of VOC oxidation on ozone production (Sillman, 1995). Also, space-based HCHO column observations are often used to constrain isoprene emissions inventories, with direct consequences for modeled ozone and SOA (Millet et al., 2008; Palmer et al., 2003). *In situ* measurements of HCHO, isoprene, and NO_x are highly resolved in space and time, allowing for their photochemical relationships to be explored in great detail (Wolfe et al., 2016a). Observations of these and several related species were collected during the Southeast Nexus (SENEX) aircraft campaign, which took place in the Southeast United States in 2013 (Warneke et al., 2016). This region is abundant in isoprene and variable in NO_x, which provides a unique opportunity to test the sensitivity of modeled HCHO to differences in isoprene chemistry.

Here, we combine *in situ* observations from SENEX with a constrained photochemical box model to evaluate and inter-compare isoprene oxidation schemes in five different gas-phase chemical mechanisms: CB05, CB6r2, GEOS-Chem, MCMv3.2, and MCMv3.3.1. The box model is constrained to observations of isoprene and related species – NO, NO_2, O_3, CO, methane (CH_4), methanol (CH_3OH), and peroxy acetyl nitrate (PAN) – and is used to simulate isoprene chemistry during SENEX with respect to each considered mechanism. *In situ* measurements of HCHO provide a benchmark for model performance, and inter-comparison of reaction-specific HCHO production rates elucidates the mechanistic drivers of model-to-model differences. Based on the results of our study, we recommend improvements to CB6r2, which has the greatest potential for impact with regard to air quality management. Implications for modeled ozone are discussed.

2. Choice of gas-phase chemical mechanisms

Mechanisms investigated in this work include two versions of

Table 1
Gas-phase chemical mechanisms evaluated and compared in this work.

Mechanism	Species	Reactions	Reference
CB05[a]	53	156	Yarwood et al., 2005
CB6r2[a]	77	216	Hildebrandt Ruiz and Yarwood, 2013
GEOS-Chem[b]	171	505	Mao et al., 2013b
MCMv3.2[c]	455	1 476	Saunders et al., 2003
MCMv3.3.1[c]	610	1974	Jenkin et al., 2015

[a] Updated for consistency with CAMx v6.40 documentation
[b] Updated for consistency with Fisher et al. (2016), Kim et al. (2015), Marais et al. (2016), and Travis et al. (2016).
[c] Subset of MCM with organic chemistry limited to methane, methanol, and isoprene oxidation.

the Carbon Bond (CB) mechanism, CB05 and CB6r2; two versions of the Master Chemical Mechanism (MCM), MCMv3.2 and MCMv3.3.1; and GEOS-Chem v9-2+. Condensed mechanisms CB05, CB6r2, and GEOS-Chem are designed for implementation in chemical transport models (CTMs): CB05 and CB6r2 are used extensively in air quality simulations (Canty et al., 2015; Goldberg et al., 2016), and GEOS-Chem is a standard tool for evaluation of space-based HCHO column observations (Zhu et al., 2016). The MCM, which is chemically near-explicit (i.e., highly detailed), is commonly used with photochemical box models to assess knowledge of tropospheric chemistry, and also provides a benchmark for evaluating condensed mechanisms (Jenkin et al., 2015). Size and complexity vary widely between mechanisms, from ~50 species and ~150 reactions in CB05 to ~600 species and ~2000 reactions in an isoprene-focused subset of MCMv3.3.1. The number of species and reactions included in each mechanism are listed in Table 1.

Each mechanism features a unique isoprene oxidation scheme. The CB05 mechanism uses a scheme carried over from CB4, in which first-generation isoprene oxidation is represented by a single reaction: isoprene reacts with OH to form HO_2, RO_2, MVK, MACR, and HCHO (Yarwood et al., 2005). Intermediate $ISOPO_2$ is not explicitly described. The isoprene scheme is updated in CB6r2 to account for the formation of $ISOPO_2$ and its reactions with NO, HO_2, and RO_2 (Hildebrandt Ruiz and Yarwood, 2013). Isomerization of $ISOPO_2$ is also represented; however, only the 1,6-H shift is considered. The isoprene scheme in GEOS-Chem v9-2+ was recently updated to include the 1,6-H shift isomerization pathway, and its basic underlying structure is similar to that of CB6r2 (Mao et al., 2013b; Travis et al., 2016). The 9-2+ version also features optimized yields of ISOPOOH and ISOPN, up-to-date secondary chemistry, and expanded treatment of SOA (Fisher et al., 2016; Kim et al., 2015; Marais et al., 2016; Travis et al., 2016). The MCMv3.2 mechanism adopts a more complex isoprene oxidation scheme that traces four different $ISOPO_2$ isomers through their reactions with NO, HO_2, and RO_2 (Saunders et al., 2003). The distribution of $ISOPO_2$ isomers and their unique products depends on the $ISOPO_2$ lifetime (Teng et al., 2017), which is neglected in coarser mechanisms. The MCMv3.2 scheme additionally considers the reaction of $ISOPO_2$ with NO_3; however, the 1,5-H shift and 1,6-H shift isomerization pathways are omitted. Both isomerization pathways are included in MCMv3.3.1, along with reversible O_2 addition to form $ISOPO_2$, new OH adducts and $ISOPO_2$ isomers, and updates to existing reaction parameters following recommendations from recent literature (Jenkin et al., 2015).

Early versions of the CB and MCM were included in a mechanism inter-comparison study by Pöschl et al. (2000), which was one of the first to focus specifically on isoprene chemistry. The purpose of the study was to develop a new condensed isoprene oxidation mechanism (Mainz Isoprene Mechanism, MIM) based on explicit chemistry in MCMv2, and to compare model performance against other condensed mechanisms, including CB4. A box model was used to simulate different emission scenarios and produce time series of several species, which were evaluated against MCMv2. Compared to MCMv2, most condensed mechanisms underestimated modeled ozone except for MIM, which agreed mostly to within 10%. Von Kuhlmann et al. (2004) implemented selected mechanisms from the Pöschl study – including MIM and CB4 – in the MATCH-MPIC (Model of Atmospheric Transport and Chemistry – Max-Planck-Institute for Chemistry) CTM. The simulated global tropospheric ozone burden was found to be relatively insensitive to choice of isoprene mechanism, varying by only 5%.

Similar studies have been performed since, but perhaps the most relevant to this work is by Archibald et al. (2010), who intercompared more recent mechanisms including CB05, GEOS-Chem v7-3-6, and MCMv3.1. Their study demonstrated good agreement with respect to modeled ozone, but large variability in modeled mixing ratios of other isoprene oxidation products such as HCHO, MVK, and MACR. Mechanisms were evaluated by comparison to MCMv3.1: most organic products were overestimated by CB05 and were either matched or underestimated by GEOS-Chem, depending on conditions for isoprene and NO_x. Zhang et al. (2011) followed with an inter-comparison of some of the same mechanisms – such as CB05 and MCMv3.1 – that included support from chamber studies. Under isoprene-rich conditions, MCMv3.1 matched measured ozone mixing ratios within 5–45%, improving with chamber evolution over time; CB05, however, consistently underestimated ozone by at least 30%. The MCM also matched peak measurements of MVK and MACR within ~20%, though a similar comparison was not included for CB05. Measurements of HCHO were not reported.

The CB, GEOS-Chem, and MCM mechanisms have all recently been updated to reflect the current understanding of isoprene chemistry. New versions CB6r2, GEOS-Chem v9-2+, and MCMv3.3.1 account for recent contributions from Paulot et al. (2009a, 2009b), Peeters et al. (2009), and many others (Bates et al., 2014; Crounse et al., 2011; Da Silva et al., 2010; Peeters and Müller, 2010; Peeters et al., 2014; Wolfe et al., 2012). Inclusion of previous versions of the CB and MCM allows us to examine the impact of these recent updates. Specific updates between GEOS-Chem v9-2+ and prior versions are discussed elsewhere (Fisher et al., 2016; Kim et al., 2015; Marais et al., 2016; Travis et al., 2016). Our study is the first isoprene-focused inter-comparison to include the most recent versions of these mechanisms, and to evaluate results by comparison to *in situ* observations of isoprene oxidation products such as HCHO.

3. Methods

3.1. Aircraft observations

The objective of the NOAA SENEX mission was to explore the interactions between biogenic and anthropogenic emissions that define atmospheric composition in the summertime Southeast US. Based out of Smyrna, TN, SENEX comprised 20 research flights of the NOAA WP-3D aircraft between May 29 and July 10 of 2013. Flight tracks are provided in Fig. 1. The payload featured instruments that characterize and quantify aerosols and numerous gas-phase atmospheric constituents including ozone, NO_x, and VOCs (Warneke et al., 2016). More information about the SENEX aircraft campaign is available at http://www.esrl.noaa.gov/csd/projects/senex/.

In situ observations of HCHO obtained during SENEX were collected using the NASA In Situ Airborne Formaldehyde (ISAF) instrument, which detects HCHO by laser-induced fluorescence (LIF) (Cazorla et al., 2015). The ISAF instrument reports measurements of HCHO at 1 Hz, and has a detection limit of 36 ppt for a signal-to-noise ratio of 2. Accuracy is ±10% based on instrument calibration, which is determined via standard additions of known HCHO mixtures to zero air before and after each field mission. As described in Cazorla et al. (2015), calibration is tied to the literature UV cross section of HCHO (Meller and Moortgat, 2000) and typically varies by less than 10% over the course of a mission. Observations of NO, NO_2, O_3, CO, isoprene, methane, methanol, PAN, and the J-values $J(O^1D)$ and $J(NO_2)$ are used to constrain the box model, which is described in the next section. Corresponding instrumentation and measurement accuracies are included in Table 2. Further information on SENEX instrumentation is provided by Warneke et al. (2016).

All observations used in this study are averaged to a 60-s time base and then filtered for daytime (SZA < 70°), boundary-layer

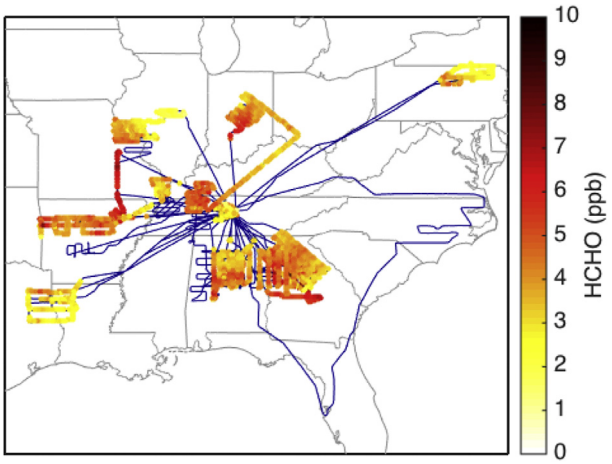

Fig. 1. Map of the flight tracks from the SENEX aircraft campaign. Flight tracks are plotted in blue, with ISAF measurements of HCHO (ppb) plotted over the tracks, according to the scheme denoted by the color bar. Observations are 60-s averages and are only included if collected in the daytime (SZA < 70°) boundary layer (altitude < 1 500 m). Observations affected by biomass burning (CO > 300 ppb or acetonitrile > 0.5 ppb), fresh NO_x sources (NO_x > 95th percentile), and missing or negative measurements of constrained species are excluded. (For interpretation of the references to color in this figure legend, the reader is referred to the web version of this article.)

(altitude < 1 500 m) conditions. Data are also filtered to exclude biomass burning (CO > 300 ppb or acetonitrile > 0.5 ppb), fresh NO_x sources (NO_x > 95th percentile), and missing or negative measurements of species used to constrain the box model. This filtering procedure retains a total of 2 219 data points, spanning a wide gradient in mixing ratios of both NO_x (0.07–1.63 ppb) and isoprene (~0–8.15 ppb). Fig. 1 shows the geographical distribution of observed HCHO mixing ratios (1.12–9.98 ppb) that are included in our analysis.

3.2. Box model simulations

We use the Framework for 0-D Atmospheric Modeling version 3 (F0AMv3) (Wolfe et al., 2016b) to simulate isoprene chemistry during SENEX. Though each simulation features a different chemical mechanism, the model setup is otherwise identical. Simulations are constrained to match observed mixing ratios of NO, NO_2, O_3, CO, isoprene, methane, methanol, and PAN, while H_2 (not observed) is assigned a mixing ratio of 550 ppb (Novelli et al., 1999). Mixing ratios are held fixed throughout each model run for all constrained species except NO, which is allowed to float after initialization to preserve the modeled NO/NO_2 ratio. Reaction rate constants are calculated using aircraft measurements of pressure, temperature, and relative humidity. Time and location of the aircraft are used to calculate solar zenith angle (SZA), which controls photolysis rates as described below. The chemical system defined by each set of observations is integrated 72 hr forward in time, in 1-hr time steps with time-varying SZA, to reach diel steady state. Physical losses are represented by a 24-hr lifetime applied to all species.

The J-values corresponding to the major photolytic pathways of ozone and NO_2 – $J(O^1D)$ and $J(NO_2)$, respectively – are constrained to match observations. All other J-values are initialized using a set of lookup tables based on literature-derived photolysis parameters and solar spectra from the NCAR Tropospheric Ultraviolet and Visible (TUV) radiation model (https://www2.acom.ucar.edu/modeling/tropospheric-ultraviolet-and-visible-tuv-radiation-model). Lookup tables are organized by SZA, altitude, overhead ozone, and surface albedo (Wolfe et al., 2016b). We use SZA and altitude from aircraft measurements and constant values for ozone column (300 DU) and surface albedo (0.05), which we estimate for SENEX using concurrent data from the Ozone Monitoring Instrument (OMI) Level-3 OMDOAO3e data product (https://disc.gsfc.nasa.gov/Aura/data-holdings/OMI/omdoao3e_v003.shtml). The average ratio of measured-to-calculated $J(O^1D)$ and $J(NO_2)$ provides a multiplicative scaling factor, which is applied to all unconstrained J-values. This scaling technique improves consistency with observations and reduces sensitivity to initial choice of overhead ozone column and surface albedo. Once initialized, all J-values are allowed to evolve throughout the corresponding model run following a simulated diel cycle.

For each simulation, model output includes diel steady-state mixing ratios and instantaneous reaction rates for species corresponding to the implemented gas-phase chemical mechanism. In the following analysis, we evaluate the isoprene schemes in the five mechanisms chosen for this study by comparing modeled HCHO mixing ratios to SENEX observations. Additionally, we explore the underlying chemistry of the mechanisms by closely examining simulated HCHO production and loss rates.

4. Analysis

4.1. Comparison to observations

To assess the accuracy of the mechanisms, we compare modeled and measured mixing ratios of HCHO from SENEX, as shown in Fig. 2. Linear least-squares regression analysis is performed for each mechanism with respect to observations, and normalized mean bias (NMB) is calculated as follows:

$$\mathrm{NMB} = \frac{\frac{1}{n}\sum_{i=1}^{n}(M_i - O_i)}{\frac{1}{n}\sum_{i=1}^{n}O_i} \times 100\% \quad (1)$$

where M is the modeled HCHO mixing ratio (ppb) and O is the observed HCHO mixing ratio (ppb) for each individual point i in a total of n data points ($n = 2\,219$). Model-measurement agreement is best for MCMv3.3.1, with a regression slope of 0.84 ± 0.01 (1σ) and an NMB of −15%. Agreement worsens among the other mechanisms in the following order: GEOS-Chem (slope = 0.83 ± 0.01; NMB = −17%), MCMv3.2 (0.73 ± 0.01; −25%), CB6r2

Table 2
Instrumentation for the SENEX observations used in this work (adapted from Warneke et al., 2016).

Measurement	Technique	Accuracy
NO; NO_2; O_3	Chemiluminescence	3%; 4%; 2%
CO	Vacuum ultraviolet resonance fluorescence	5%
CH_4	Cavity ring-down spectroscopy (CRDS)	0.07 ppm
C_5H_8; CH_3OH	Proton-transfer-reaction mass spectrometry (PTR-MS)	25%
HCHO	Laser-induced fluorescence (LIF)	10%
PAN	Chemical ionization mass spectrometry (CIMS)	0.04–0.05 ppb
J-values	Filter radiometry	10%

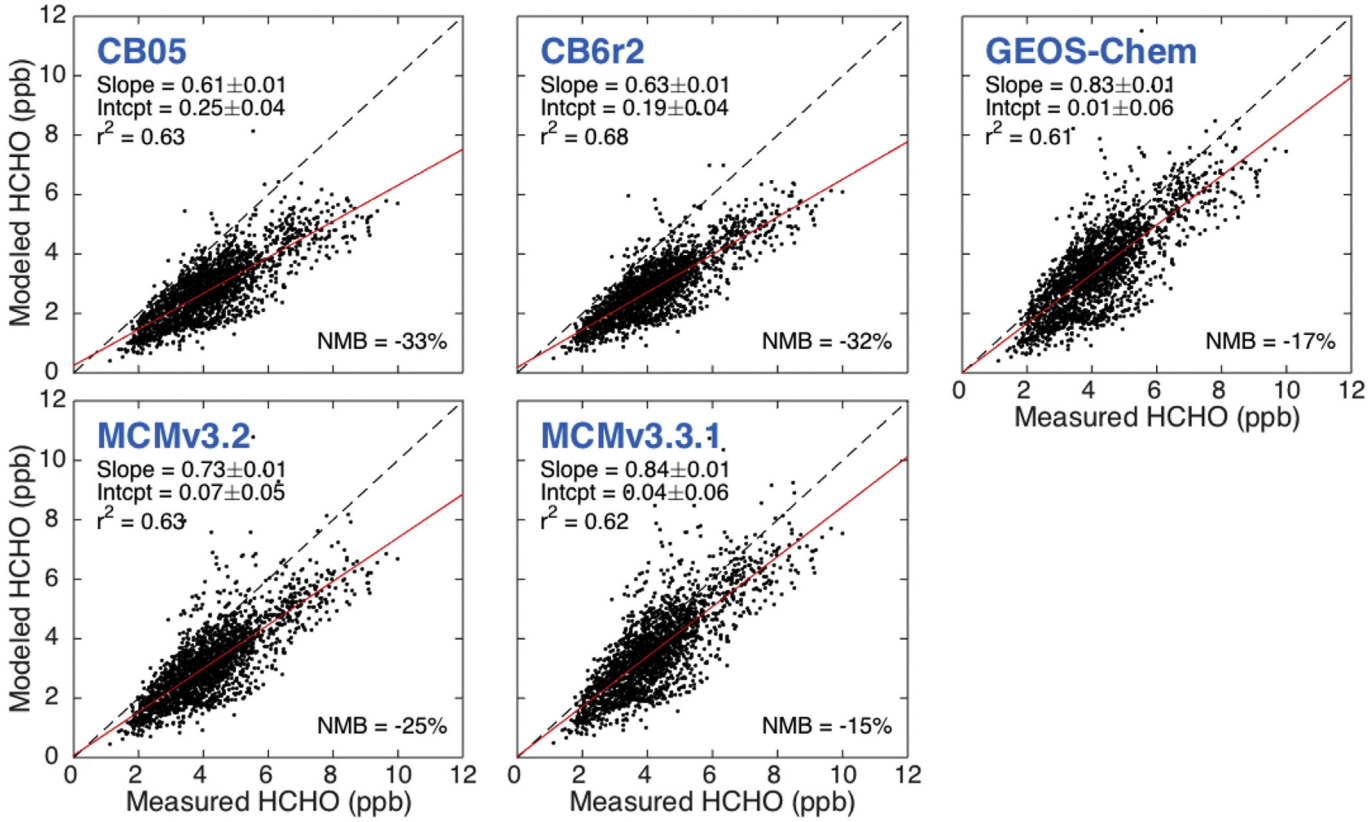

Fig. 2. Regression of modeled and measured mixing ratios of HCHO (ppb) from SENEX. Each panel features HCHO modeled using a different gas-phase chemical mechanism, as indicated. In each case, linear least-squares regression analysis provides parameters for a line of best fit, which is plotted in red. The 1:1 line, shown here as a dashed black line, is provided for reference. All uncertainties are 1σ standard deviations. (For interpretation of the references to color in this figure legend, the reader is referred to the web version of this article.)

(0.63 ± 0.01; −32%), and CB05 (0.61 ± 0.01; −33%). Using a two-tailed Z-test, we determine that differences in the slopes are statistically significant (p-value < 0.05), except between GEOS-Chem and MCMv3.3.1 (p-value = 0.56). Calculated r^2 values range from 0.61 for GEOS-Chem to 0.68 for CB6r2, indicating that 60–70% of the variability in the data is reproduced by the model. The fact that the r^2 values are all very similar suggests that any unexplained variability is consistent among mechanisms and does not significantly influence differences in modeled HCHO. The MCMv3.3.1 and CB6r2 mechanisms demonstrate improved agreement with observations over their predecessors (MCMv3.2 and CB05, respectively); however, the degree of improvement of CB6r2 over CB05 is low, which is perhaps surprising given the drastic changes in the isoprene oxidation chemistry between these two CB versions. The chemically explicit MCM mechanisms result in better agreement with observations than either of the mechanisms of the condensed CB, though GEOS-Chem performs nearly as well as MCMv3.3.1, despite its classification as a condensed mechanism.

Comparison to observations also enables evaluation of the overall relationship between HCHO, isoprene, and NO_x. Fig. 3 shows the NO_x-dependence of measured and modeled HCHO from SENEX. Observations demonstrate a trend of increasing HCHO with NO_x, which is captured by all five mechanisms. As noted by Wolfe et al. (2016a), changes in both OH production and RO_2 branching drive this trend, with the former having a stronger net influence. The strength of the observed NO_x-dependence (Δy/Δx between endpoints ~ 2.75 ppb HCHO per log(NO_x (ppb))) is best reproduced by MCMv3.2 (2.78). Otherwise, modeled NO_x-dependences vary in strength from CB05 (1.67) to MCMv3.3.1 (3.00). A more complex isoprene scheme in CB6r2, which includes NO-dependent branching of isoprene-derived RO_2 radicals, results in a stronger NO_x-dependence than is modeled for CB05. As a result, CB05 agrees better with measurements of HCHO obtained under low-NO_x conditions, but CB6r2 agrees better at high NO_x. Similarly, differences in the strengths of the NO_x-dependences of GEOS-Chem and

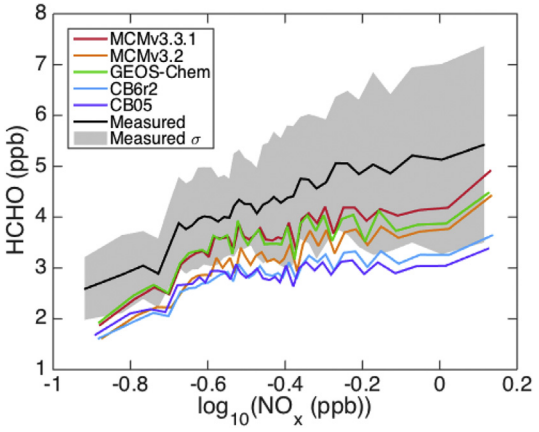

Fig. 3. NO_x-dependence of HCHO (ppb), as measured (black) and modeled (colors, as indicated for each mechanism) for SENEX. Data and model output are binned by log(NO_x), with each bin containing 60 points. Lines represent bin averages; the grey shaded region is the 1σ standard deviation of the binned measurements, which is not shown for the binned model output. (For interpretation of the references to color in this figure legend, the reader is referred to the web version of this article.)

MCMv3.3.1 allow GEOS-Chem to match MCMv3.3.1 at low NO_x, but to underestimate at high NO_x. This behavior is partly explained by the NO_x-dependence of modeled OH (Fig. S1 in the Supplement): larger mixing ratios of OH at high NO_x in MCMv3.3.1 increase production of HCHO. Higher mixing ratios of OH also partly explain the ~0.5 ppb increase in modeled HCHO between MCMv3.2 and MCMv3.3.1, which is independent of NO_x across the range of conditions presented in Fig. 3. For all mechanisms, model-measurement agreement tends to decline with increasing NO_x and demonstrates nonlinear behavior at the tail ends of the NO_x distribution (Fig. S2).

Although most mechanisms effectively simulate the NO_x-dependence of HCHO, none reproduce the magnitude of measured HCHO mixing ratios. Fig. 2 points to a systematic bias in modeled HCHO that, in Fig. 3, is shown to be consistent across NO_x regimes. For all five simulations, HCHO is underestimated by at least 0.5–1 ppb throughout the range of NO_x conditions sampled during SENEX. These results mirror those of Wolfe et al. (2016a), who observed the same trend in MCMv3.3.1 as well as the global model AM3 (Donner et al., 2011), which runs using a self-contained gas-phase chemical mechanism with updated isoprene chemistry (Mao et al., 2013a; Naik et al., 2013). Underestimated HCHO in both the 0-D and global models suggests that this bias is not an artifact of the steady-state box model setup. Wolfe et al. attributed the bias to "background" HCHO, due to either missing primary VOCs or inadequate representation of HCHO production in the later generations of isoprene degradation. Investigation of background HCHO from late-generation isoprene oxidation would require observations to constrain the full scope of the isoprene cascade, such as OH reactivity or additional late-generation products. However, we explore the impact of non-methane, non-isoprene primary VOCs on background HCHO in Section 4.3 and investigate additional strategies for bias mitigation in Section 5.

4.2. Formaldehyde production rates

To understand differences in simulated HCHO, we intercompare underlying chemical rates. Because the lifetime of HCHO is comparable across all mechanisms (within 7%), our analysis focuses primarily on rates contributing to HCHO production. Average HCHO production rates (ppb hr^{-1}) computed for SENEX are shown in Fig. 4. Total rates range from 1.30 to 1.77 ppb hr^{-1}. Individual rates are sorted by primary source VOC – methane, methanol, or isoprene – and rates specific to isoprene chemistry are further classified by the product generation in which HCHO is formed. 'Other' accounts for HCHO production from late-generation isoprene oxidation by OH, including PAN degradation, and from isoprene oxidation by O_3, $O(^3P)$, and NO_3. Grouping individual rates is complex, as many reactions are common to different VOCs or are multi-generational. A description of our grouping scheme and a list of group assignments are provided in the Supplement (Section S1 and Table S1).

The formulation of CB6r2 expands the simple isoprene scheme in CB05 to consider the NO_x-dependent reactivity of $ISOPO_2$ (Hildebrandt Ruiz and Yarwood, 2013). Fig. 4 shows that the updated chemistry increases the average production of HCHO by 0.06 ppb hr^{-1} (~5%), consistent with increased HCHO mixing ratios (Fig. 2). Formaldehyde production from first- and second-generation isoprene oxidation is actually reduced by 0.13 ppb hr^{-1} within CB6r2. Increases in the production of HCHO are attributed to methane, methanol, and late-generation isoprene oxidation chemistry. The increases from methane and methanol oxidation result from more efficient radical recycling: additional OH and HO_2 are returned to the system by new RO_2 reaction pathways and new isoprene oxidation products, such as HPALD. Increased recycling of both species leads to larger modeled mixing ratios of OH (Fig. S1), effectively increasing production of HCHO. Other updates within CB6r2 include the addition of new isoprene oxidation products – such as IEPOX and glycolaldehyde (GLYD) – that form HCHO in later generations. Several existing reactions were updated to add or increase formation of methyl peroxy radical (CH_3O_2), a major source of late-generation HCHO. The CH_3O_2 radical is also formed via $RO_2 + RO_2$ chemistry, which is expanded in CB6r2 to account for new RO_2 species – such as $ISOPO_2$ and $IEPOXO_2$ – increasing the contribution to late-generation HCHO production even further. However, the cumulative increases in HCHO production from late-generation isoprene chemistry barely outweigh the reductions from first- and second-generation chemistry, explaining why modeled HCHO rises so little between CB05 and CB6r2.

The MCMv3.3.1 mechanism builds on the complex isoprene scheme of MCMv3.2 and refines the chemistry for consistency with several recent laboratory and theoretical studies (Jenkin et al., 2015). The applied updates increase the average production of HCHO by 0.25 ppb hr^{-1} (~16%) between MCMv3.2 and MCMv3.3.1. New radical chemistry, $ISOPO_2$ isomers, and $ISOPO_2$ isomerization pathways in MCMv3.3.1 increase first-generation HCHO production from isoprene oxidation. Representation of minor OH-adducts in MCMv3.3.1 yields new first-generation oxidation products pent-4-en-2-one and 3-methyl-but-3-enal, which react to form HCHO in the second generation. Though the chemistry of these species is largely based on theory (Park et al., 2003), it accounts for ~2% of total HCHO production in MCMv3.3.1 and ~88% of the increase in second-generation HCHO production between MCMv3.2 and MCMv3.3.1. Updates to the late-generation isoprene oxidation chemistry, however, are responsible for the largest increases in HCHO production, totaling 0.14 ppb hr^{-1}. For example, MCMv3.3.1 includes several new or enhanced sources of acetyl peroxy radical (CH_3CO_3), a precursor of PAN and CH_3O_2; furthermore, updated rate constants controlling PAN equilibria increase production of CH_3CO_3 from PAN by a factor of 2. These changes lead to increased production of CH_3O_2, and therefore HCHO, in the late stages of isoprene oxidation. Finally, larger OH mixing ratios in MCMv3.3.1 from additional radical recycling – mainly via RO_2 isomerization and HPALD photolysis – increase the production of HCHO from all source VOCs.

Though considered a condensed mechanism, GEOS-Chem v9-2+ contains a detailed isoprene scheme that was recently updated to incorporate results from a variety of studies (Fisher et al., 2016; Kim et al., 2015; Marais et al., 2016; Travis et al., 2016). Consequently, the average production of HCHO during SENEX approaches that of MCMv3.3.1 (1.68 and 1.77 ppb hr^{-1}, respectively), differing by only ~5%. The distribution of HCHO sources is also very similar. Cumulative production of HCHO from methane, methanol, and first-generation isoprene oxidation matches within 5%. However, GEOS-Chem exhibits more second-generation and less late-generation HCHO production compared to MCMv3.3.1. Because the representation of underlying chemistry is fundamentally different between condensed and explicit mechanisms, it is difficult to pinpoint causes of discrepancy. Nevertheless, broad comparison of major HCHO-producing reactions allows us to make some determinations. For instance, HPALD photolysis is a much larger source of HCHO in GEOS-Chem than in MCMv3.3.1. Since J-values are consistent between simulations (Section 3.2), we attribute this discrepancy to differing yields of HCHO and HCHO precursors. Furthermore, HCHO production from HPALD photolysis is prompt (second-generation) in GEOS-Chem but delayed (late-generation) in MCMv3.3.1 due to formation of intermediate VOCs. The treatment of HPALD photolysis in GEOS-Chem thus contributes to more production of HCHO in the second generation. Late-generation

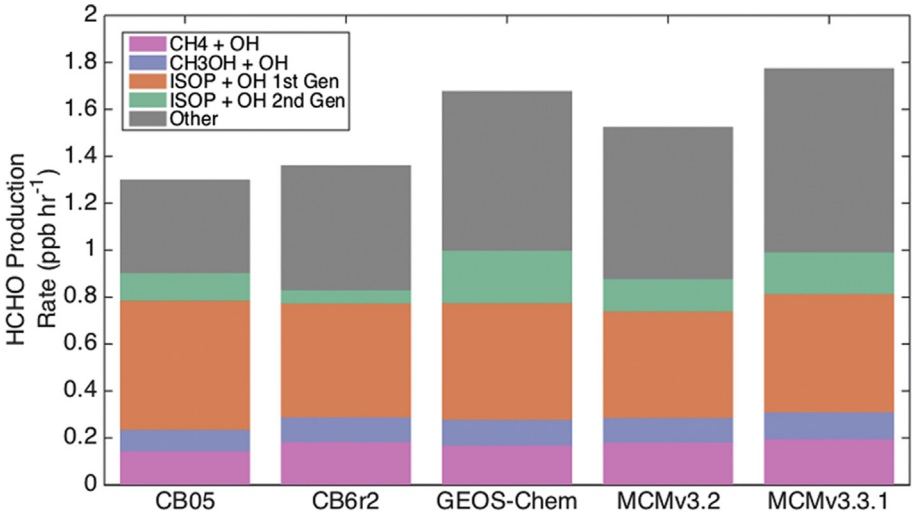

Fig. 4. Average HCHO production rates (ppb hr^{-1}) simulated for SENEX. Rates are grouped by contribution to HCHO production from methane, methanol, and isoprene oxidation (first- and second-generation). 'Other' accounts for HCHO production from late-generation isoprene oxidation by OH, including PAN degradation, and from multi-generational isoprene oxidation by O_3, $O(^3P)$, and NO_3.

HCHO production is limited by the production of CH_3O_2, which is 10% less in GEOS-Chem than in MCMv3.3.1. An evaluation of the CB mechanisms with respect to MCMv3.3.1 is presented in Section 5.

Differences in the generational distribution of HCHO production rates lead to discrepancies in the time-evolution of modeled HCHO (Fig. S3). A prior study by Marais et al. (2012) investigated the simulated yield of HCHO from isoprene oxidation as a function of time and under varying conditions for NO_x. We apply a similar approach to explore the temporal behavior of each of the five mechanisms considered in this work, and we find that modeled HCHO and its time progression vary between mechanisms and NO_x conditions, as in Marais et al. The influence of the distribution of HCHO production rates is manifested in the rate of change of HCHO mixing ratios throughout subsequent diel cycles. Though the mechanisms tend to deviate over time in all NO_x regimes, the greatest variation (~0.5 cumulative ppb HCHO per ppb initial isoprene) occurs in the high-NO_x simulation (1 ppb), which favors production of tropospheric ozone. Precisely representing the time-evolution of isoprene oxidation products such as HCHO and ozone is critical for effective air quality modeling.

4.3. Uncertainties

As described in Section 3.1, the stated accuracy of ISAF HCHO is ±10%. This estimate comprises calibration uncertainty but does not account for interference from ISOPOOH, which has been shown to affect ISAF measurements of HCHO (St. Clair et al., 2016). Measurements of $C_5H_{10}O_3$ (lumped ISOPOOH and IEPOX) were obtained during SENEX via chemical ionization mass spectrometry (CIMS) (Warneke et al., 2016). Applying an ISOPOOH-to-HCHO conversion rate of 6%, which is recommended for ISAF under SENEX-like conditions (St. Clair et al., 2016), we determine that ISOPOOH interference inflates measured HCHO by at most ~1% on average. A systematic 11% down-revision in observed HCHO mixing ratios, derived from combining calibration uncertainty and ISOPOOH interference, would not be sufficient to bring measured and modeled HCHO into agreement.

Modeled HCHO is also subject to uncertainty, which can arise from errors in the observational constraints. Stated accuracies for measurements of most constrained species are within 5% (Table 2), and we expect these uncertainties to have a minimal impact on modeled HCHO. However, larger uncertainties are reported for PAN (0.04–0.05 ppb, ~15%) and VOCs (25%), including isoprene and methanol. Sensitivity simulations suggest that systematic error in constrained PAN or methanol could explain about 10% of the discrepancy between measured and modeled HCHO, whereas error in constrained isoprene could account for nearly 50%. Depending on the mechanism used, the combination of a 25% increase in constrained isoprene with an 11% decrease in measured HCHO could bring model and measurements into agreement. However, the required correction of isoprene observations is not supported by recent instrument inter-comparison studies (Lerner et al., 2017; Warneke et al., 2016).

Modeled HCHO may also be limited by the choice of represented sources. Although HCHO is a pervasive byproduct of general VOC oxidation, our box model setup assumes that primary VOCs isoprene, methane, and methanol dominate the photochemical production of HCHO in the Southeast US. To test this assumption, we perform a simulation constrained to observations of primary VOCs collected by the improved whole air sampler (iWAS) during SENEX. The iWAS provides observations of 24 primary VOCs, including a variety of alkanes, alkenes, aromatics, and monoterpenes (Lerner et al., 2017; Warneke et al., 2016). Using the MCMv3.3.1 mechanism, which resolves explicit chemistry for most measured VOCs, we find that omission of observed primary VOCs explains <10% of the difference between modeled and measured HCHO. Observations of secondary VOCs MVK and MACR were also collected during SENEX, measured via iWAS analysis and proton-transfer-reaction mass spectrometry (PTR-MS). As first-generation products of isoprene oxidation, these species are useful in constraining HCHO production in later generations. However, the two sets of measurements do not agree, with lumped MVK and MACR measured ~30% higher by iWAS analysis (Lerner et al., 2017). Greater benefit to modeled HCHO is achieved by constraining to iWAS MVK and MACR, which improves model-measurement agreement by ~10%; however, due to potential ISOPOOH interference (Rivera-Rios et al., 2014), this effect is likely overestimated. We do not constrain to iWAS observations in the base model runs because iWAS sampling severely limits the size of our dataset ($n = 62$), but we conclude that, within measurement uncertainties, inclusion of all observed VOCs still cannot explain the HCHO model-measurement discrepancy.

Photochemical rate constants provide another source of model uncertainty. Based on our box model setup, photolysis frequencies are limited by uncertainties in constrained J-values (10%). Kinetic rate constants, on the other hand, are unique to each mechanism and are generally drawn from established databases such as the IUPAC Task Group on Atmospheric Chemical Kinetic Data Evaluation (http://iupac.pole-ether.fr/) or the JPL Data Evaluation (http://jpldataeval.jpl.nasa.gov/). Such databases combine information from laboratory and chamber studies to determine the "preferred value" of each rate constant. Uncertainties from the individual studies and their combination lead to uncertainties in the preferred values. Following the procedure described in Section S2, we estimate that uncertainty in photochemical rate constants produces ~12% (1σ) uncertainty in modeled HCHO mixing ratios for each of our box model simulations. This error is random and could imply better, or worse, model-measurement agreement than is indicated in Section 4.1.

5. Suggested modifications to CB6r2

The two mechanisms geared specifically towards air quality simulations, CB05 and CB6r2, underestimate HCHO by 33% and 32%, respectively. These results imply deficiencies in the same coupled chemical system that predicts ozone and SOA. Although CB05 is still widely used today, its isoprene scheme cannot be easily improved without first upgrading to CB6r2. The CB6r2 mechanism contains more developed isoprene chemistry and is thus more suitable for incorporating modifications. Here we present suggestions for improving simulated HCHO in CB6r2 and consider effects on modeled ozone.

We evaluate HCHO production rates in CB6r2 using MCMv3.3.1 as a benchmark. Average production of HCHO during SENEX is considerably lower in CB6r2 compared to MCMv3.3.1 (1.36 and 1.77 ppb hr^{-1}, respectively). Fig. 4 shows that cumulative production of HCHO from methane, methanol, and first-generation isoprene oxidation is comparable between CB6r2 and MCMv3.3.1, with the two values differing less than 5%. However, the production of HCHO from second- and late-generation isoprene oxidation is underestimated by CB6r2, relative to MCMv3.3.1, by a factor of 1.64. We find that CB6r2 omits HCHO production from both the 1,5-H shift and 1,6-H shift pathways of $ISOPO_2$ isomerization; in MCMv3.3.1, the 1,5-H shift pathway contributes to first-generation HCHO production, the 1,6-H shift pathway to late-generation HCHO production. The CB6r2 mechanism also omits HCHO from the OH oxidation of MVK and MACR, a source of second-generation HCHO in MCMv3.3.1. Finally, CB6r2 omits or underestimates HCHO production from several late-generation reactions, including the OH oxidation of GLYD and the radical reactions of $IEPOXO_2$.

We recommend a set of modifications (Table 3) to address the underestimated production of HCHO in the second and late generations of isoprene oxidation within CB6r2. Modification 1 is intended to correct missing HCHO from $ISOPO_2$ isomerization. The existing 1,6-H shift pathway in CB6r2 produces HPALD and HO_2; subsequent HPALD photolysis forms MVK, MACR, and OH. Production of HCHO via 1,6-H shift isomerization is complex in MCMv3.3.1, so we look to GEOS-Chem for a condensed representation. Following v9-2+, we add HCHO to the products of HPALD photolysis with a yield of 100%. Though GEOS-Chem also includes production of HCHO from HPALD oxidation, the proposed modification to CB6r2 results in about the same average HCHO production as the combined HPALD reactions in GEOS-Chem (0.11 and 0.08 ppb hr^{-1}, respectively). Production of HCHO via 1,5-H shift isomerization of $ISOPO_2$ is also expected. However, representation of this pathway in MCMv3.3.1 accounts for a small fraction of total HCHO production (~1%), and we refrain from adding entirely new reactions to CB6r2 due to the complications of implementing such changes in CTMs. All of the other recommended modifications are supported by related studies. For example, including HCHO production from the OH oxidation of MVK and MACR (Modification 2) and the OH oxidation of GLYD (Modification 3) is consistent with the isoprene oxidation scheme proposed by Paulot et al. (2009a), upon which the isoprene chemistry of CB6r2 is based (Hildebrandt Ruiz and Yarwood, 2013). Modification 4 derives from the recent work of Bates et al. (2014), who discovered new products of IEPOX oxidation (C_4 hydroxy dicarbonyl and C_4 dihydroxy carbonyl compounds), which upon subsequent reaction, are thought to form HCHO. Finally, Modification 5 simply applies the most recent evaluation of the PAN equilibrium rate constants from IUPAC (Atkinson et al., 2006) (corresponding data sheets at http://iupac.pole-ether.fr/htdocs/datasheets/pdf/ROO_14_CH3CO3_NO2_M.pdf and http://iupac.pole-ether.fr/htdocs/datasheets/pdf/ROO_15_CH3C(O)O2NO2_M.pdf).

The recommended modifications require only minor adjustments to the existing CB6r2 mechanism (Table S2). We refer to the adjusted CB6r2 as 'CB6r2-UMD.' As shown in Fig. 5, modeled HCHO improves significantly in CB6r2-UMD relative to CB6r2. Panel a) shows a scatter plot of modeled HCHO (ppb) versus measured HCHO (ppb). Linear regression yields a line of best fit with a slope of 0.83 ± 0.01, and we calculate an NMB of −14%, which indicates that model-measurement agreement is comparable to MCMv3.3.1. Panel b) shows that average HCHO production increases 0.36 ppb hr^{-1} (~26%) in CB6r2-UMD relative to CB6r2, and that the total production rate of HCHO is within ~3% of MCMv3.3.1. The distribution of HCHO production rates among source VOCs roughly imitates that of MCMv3.3.1: Modifications 1 and 2 contribute to HCHO production from second-generation isoprene oxidation, whereas Modifications 3 through 5 contribute to HCHO production in later generations. Our proposed CB6r2-UMD mechanism thus effectively simulates the isoprene-HCHO relationship of more complex mechanisms while retaining the computational efficiency of CB6r2.

Although CB6r2-UMD improves modeled HCHO compared to other mechanisms, it is still biased low by 14% compared to measured mixing ratios of HCHO from SENEX. This deficit is consistent with our findings from Section 4.1, which revealed a negative bias in modeled HCHO relative to observations, common to all considered mechanisms. Potential sources of this bias, discussed in Sections 4.1 and 4.3, are difficult to evaluate using a box model. However, we leverage our CB6r2-UMD simulation to determine whether we can reduce the bias through the manipulation of mechanism reaction rates, within accepted uncertainties. We begin by identifying the reactions in CB6r2-UMD to which modeled HCHO is most sensitive (Section S2 and Table S3). Of these, only the thermal degradation of PAN has enough influence on modeled HCHO to eliminate model-measurement bias when the corresponding rate constant is perturbed within its 2σ uncertainty limits; however, model-measurement agreement is not achieved for HCHO or PAN, when PAN is unconstrained (Fig. S4). The next most important reaction is the OH oxidation of HCHO, which must be perturbed by a factor of 2 – significantly past its 2σ rate constant uncertainty limits (~20% at 298 K) – to match modeled and measured mixing ratios of HCHO (not shown). These results suggest that the detected bias in modeled HCHO cannot be corrected by a simple adjustment of rate parameters, but rather that continued investigation is required to isolate its cause and formulate meaningful solutions.

As we are still unable to match simulated HCHO mixing ratios to observations, we perform a CB6r2-UMD simulation constrained to measured mixing ratios of HCHO from SENEX, which allows us to assess consequences for the calculated production rate of

Table 3
Recommended modifications to CB6r2 that are incorporated into CB6r2-UMD. The parameter ΔP_{HCHO} quantifies the effect of each modification on the average HCHO production rate from SENEX.

Mod.	Description	ΔP_{HCHO} (ppb hr^{-1})	ΔP_{HCHO} (%)
1	Add HCHO as a product of HPALD + hν	0.11	8
2	Add HCHO as a product of MVK + OH and MACR + OH	0.07	5
3	Add HCHO as a product of GLYD + OH	0.05	4
4	Increase product fraction of HCHO in $IEPOXO_2$ + HO_2 and $IEPOXO_2$ + NO	0.05	4
5	Update PAN equilibrium rate constants according to IUPAC 2014	0.07	5
All	Implement Modifications 1–5 simultaneously	0.36	26

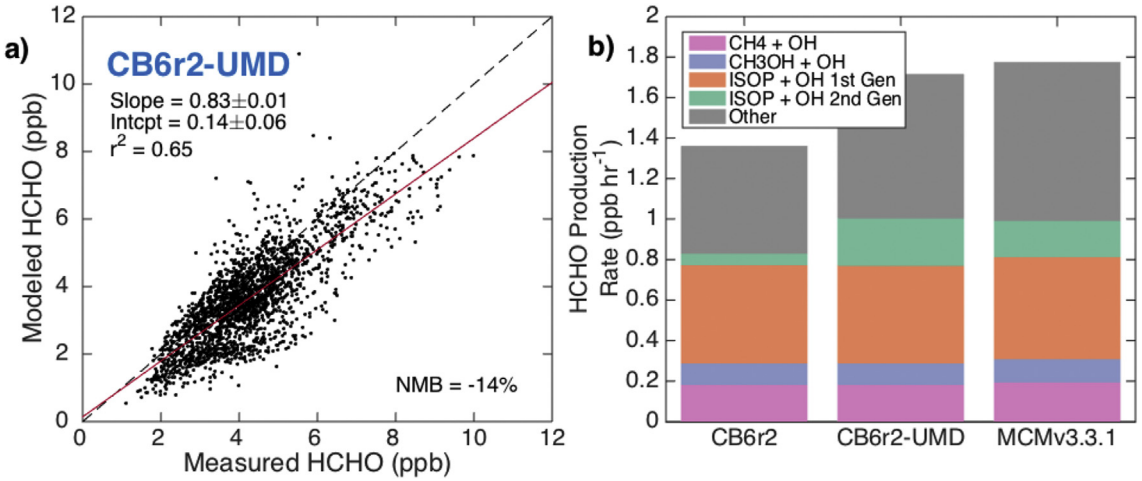

Fig. 5. a) Regression of modeled and measured mixing ratios of HCHO (ppb) from SENEX, where HCHO is modeled using CB6r2-UMD. Linear least-squares regression analysis provides parameters for a line of best fit, which is plotted in red. The 1:1 line, shown here as a dashed black line, is provided for reference. All uncertainties are 1σ standard deviations. b) Average HCHO production rates (ppb hr^{-1}) simulated for SENEX using CB6r2, CB6r2-UMD, and MCMv3.3.1. Rates are grouped by contribution to HCHO production from methane, methanol, and isoprene oxidation (first- and second-generation). 'Other' accounts for HCHO production from late-generation isoprene oxidation by OH, including PAN degradation, and from multi-generational isoprene oxidation by O_3, $O(^3P)$, and NO_3. (For interpretation of the references to color in this figure legend, the reader is referred to the web version of this article.)

tropospheric ozone. Formaldehyde degrades to form HO_2, which leads to production of ozone in the presence of NO_x. Changes in HCHO, therefore, impact the first term in the following equation for ozone production:

$$P(O_3) = k_{HO2+NO}[HO_2][NO] + \sum k_{RO2i+NO}[RO_{2i}][NO] \quad (2)$$

where $P(O_3)$ is the ozone production rate (molecules cm^{-3} s^{-1}), k_{HO2+NO} and $k_{RO2i+NO}$ are reaction rate constants (cm^3 $molecule^{-1}$ s^{-1}), and $[HO_2]$, $[RO_{2i}]$, and [NO] are species concentrations (molecules cm^{-3}). The subscript *i* denotes the separation of RO_2 into individual species for calculation of the second term. Fig. 6 illustrates how ozone production responds to differences in modeled HCHO. Ozone production rates (in ppb hr^{-1}) are calculated for SENEX using model output from the CB6r2, CB6r2-UMD, and constrained CB6r2-UMD simulations. These are then plotted as a function of NO (ppb). Increased mixing ratios of HCHO strengthen the NO-dependence of the ozone production rate, increasing ozone production at ~0.3 ppb NO by 0.24 ppb hr^{-1} (~3%) between CB6r2 and CB6r2-UMD and 0.38 ppb hr^{-1} (~4%) between CB6r2-UMD and the constrained CB6r2-UMD simulation. The "missing HCHO" represented by the constrained simulation implies a deficit of VOC oxidation, affecting all of the mechanisms investigated in this study, that directly impacts the production of tropospheric ozone.

Chemical transport models tend to overestimate surface ozone in the summertime Southeast US (Canty et al., 2015; Fiore et al., 2003; Reidmiller et al., 2009). In a recent study, Travis et al. (2016) investigated this phenomenon using the GEOS-Chem CTM with v9-2+ chemistry. Their study supports the recent discovery that non-power plant NO_x emissions are overestimated in most CTMs (Anderson et al., 2014; Castellanos et al., 2011; Fujita et al., 2012), and shows that reducing mobile and industrial NO_x emissions by 60% improves agreement between modeled and measured ozone mixing ratios at the surface. However, their model remains

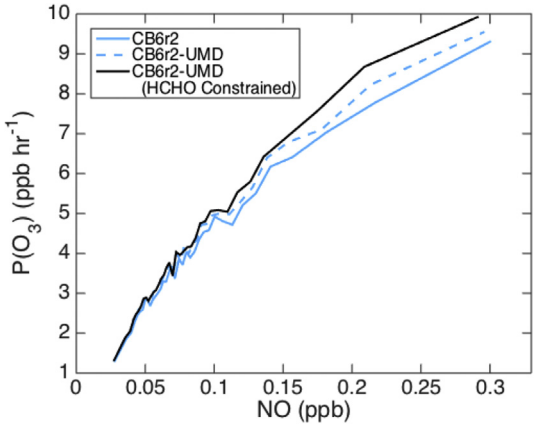

Fig. 6. Ozone production rate (ppb hr^{-1}) as a function of NO (ppb) calculated for SENEX using model output from three different simulations: CB6r2 (blue), CB6r2-UMD (blue dashed), and CB6r2-UMD constrained to observations of HCHO (black). Calculated rates are binned by NO, with each bin containing 60 points. Lines represent bin averages. (For interpretation of the references to color in this figure legend, the reader is referred to the web version of this article.)

biased high by 6 ± 14 ppb, which Travis et al. attribute to excessive vertical mixing and undiagnosed ozone chemistry. Our results show that improving modeled HCHO in the summertime Southeast US increases simulated ozone production by up to ~7%. These results are representative of boundary layer conditions; however, excessive vertical mixing may well extend the influence of our modifications to the surface, potentially worsening agreement between modeled and measured ozone mixing ratios. The resulting discrepancy in surface ozone is expected to be partly balanced by implementation of halogen chemistry (Sherwen et al., 2016). But despite the potential ramifications for modeled ozone mixing ratios, our proposed changes demonstrate improved model representation of ozone precursors, which are important in the development of air quality policy.

As a final note, two new revisions to the CB6 mechanism have been recently released: CB6r3 and CB6r4. Updates in CB6r3 account for the temperature-dependence of alkyl nitrate yields, which improves simulated ozone production rates at low temperatures, for example during wintertime (Emery et al., 2015). The subsequent revision, CB6r4, incorporates the same updates from CB6r3, removes VOC oxidation by $O(^3P)$, includes pseudo-heterogeneous hydrolysis of ISOPN, and adds a 16-reaction condensed iodine mechanism (Environ, 2016). We have performed SENEX simulations using both CB6r3 and CB6r4 (excluding halogen chemistry), and we find that the changes incorporated into each revision have a negligible (<1%) impact on modeled HCHO mixing ratios compared to CB6r2 (Fig. S5). We deduce that our suggested modifications put forth for CB6r2 apply also to CB6r3 and CB6r4, and for the summertime Southeast US, will produce nearly identical results with respect to simulated HCHO and its contribution to the production of tropospheric ozone.

6. Conclusions

In situ observations and a constrained 0-D box model were used to evaluate and inter-compare the isoprene schemes of the CB05, CB6r2, GEOS-Chem, MCMv3.2, and MCMv3.3.1 gas-phase chemical mechanisms. Comparison of modeled HCHO to measurements obtained during SENEX showed that, in general, mechanisms containing more developed isoprene oxidation chemistry (e.g., chemically explicit or recently updated) tend to simulate HCHO more accurately; however, all mechanisms were found to underestimate measured HCHO by at least 15%. The GEOS-Chem mechanism, which is used to estimate isoprene emissions from remote measurements of HCHO, achieves relatively high model-measurement agreement with an NMB of −17%. The CB05 and CB6r2 mechanisms, though often used in air quality simulations, underestimate measured HCHO by 33% and 32% respectively, which directly impacts modeled ozone.

Inter-comparison of reaction rates revealed that major restructuring of the CB isoprene scheme produces cancelling effects on HCHO production rates, so that the average production of HCHO simulated for SENEX increases only ~5% from CB05 to CB6r2. In contrast, further refinement of the complex MCM scheme increases average production of HCHO by ~16%, leading to larger modeled HCHO mixing ratios in MCMv3.3.1 relative to MCMv3.2. The GEOS-Chem mechanism, though considered condensed, provides a good approximation of the explicit isoprene chemistry in MCMv3.3.1, and reproduces average HCHO production rates within ~5%. Cumulative HCHO production from methane, methanol, and first-generation isoprene oxidation chemistry is fairly consistent between all five mechanisms, but responds to changes in radical recycling. Disagreement in the simulated production of HCHO is mainly attributed to second- and late-generation isoprene oxidation chemistry, which varies between mechanisms according to level of detail and inclusion of updates from relevant studies.

We recommend improvements to CB6r2, which has the greatest potential to impact air quality management. Evaluation of CB6r2 against MCMv3.3.1 exposed shortcomings in the isoprene scheme of CB6r2 that limit the amount of HCHO produced via isoprene oxidation. Based on these shortcomings, we proposed a few simple modifications to CB6r2 (Table 3), referred to as CB6r2-UMD, that mimicked HCHO production in MCMv3.3.1 and improved agreement with SENEX observations to −14%. These modifications are intended for implementation in CTMs, which remains to be tested. The CB6r2 and CB6r4 mechanisms are currently publicly available for use within the Comprehensive Air Quality Model with Extensions (CAMx) (http://www.camx.com/), and CB6r3 accompanied the recent release of version 5.2 of the Community Multiscale Air Quality (CMAQ) model (https://www.cmascenter.org/cmaq/). Implementation of CB6r2-UMD in a CTM such as CAMx or CMAQ will provide a means to assess the effects of improved simulation of HCHO on regional air quality modeling.

While CB6r2-UMD demonstrates improvement in the simulation of HCHO, it still underestimates measured mixing ratios by 14%, which is consistent with a negative bias affecting all of the gas-phase chemical mechanisms considered in this study. We do not propose a solution to correct this bias, but rather acknowledge its presence and recommend continued investigation. Lacking a simulation that matches measured HCHO mixing ratios, we performed a simulation constrained to observed HCHO from SENEX to assess consequences for modeled ozone. Increased production of HCHO in CB6r2-UMD relative to CB6r2 increased the production of ozone by ~3% at 0.3 ppb NO; ozone production increased another ~4% when constrained to observed HCHO. The ozone production rates reported here are averaged across the SENEX campaign, which may dampen effects in high-NO_x urban regions where nonlinearities in the ozone chemistry could lead to a stronger dependence on HCHO. Individual case studies in combination with ozone sensitivity tools may provide a more precise characterization of the relationship between HCHO and ozone in these areas.

We conclude by noting that we are generally reassured by how well the various mechanisms simulate isoprene oxidation products such as HCHO and ozone. Isoprene oxidation chemistry is extremely complex, and implementation in air quality models is complicated by the need to have a computationally efficient scheme, given the high spatial and temporal resolution of typical CTM runs. The scientific understanding of isoprene oxidation chemistry is constantly evolving, and the development of atmospheric models is an ongoing process. Current gas-phase chemical mechanisms exhibit considerable skill in simulating observed HCHO. Though presently biased low, these mechanisms improve with each revision and continue to approach agreement with observations.

Acknowledgements

We are very grateful to the SENEX team for enabling the mission and providing processed data. We thank contributors to the various mechanisms and components of the F0AM box model, including Jin Liao. Thanks also to Daniel C. Anderson and Greg Porter, who provided feedback essential to the development of this manuscript. This work was supported by NASA under several funding programs, including the Earth and Space Science Fellowship (ESSF) program (NNX15AN84H), the Atmospheric Composition Campaign Data Analysis and Modeling (ACCDAM) program (NNX14AP48G), the Atmospheric Chemistry Modeling and Analysis Program (ACMAP), and the Modeling, Analysis, and Prediction (MAP) program (NNH12ZDA001N). The SENEX WP-3D mission was supported by NOAA via the Climate Program Office and the Atmospheric

Chemistry, Carbon Cycle, and Climate (AC4) program. Support for HCHO measurements was provided by the EPA under the Science to Achieve Results (STAR) program (83540601). This research has not been subjected to any EPA review and therefore does not necessarily reflect the views of the agency, and no official endorsement should be inferred.

Appendix A. Supplementary data

Supplementary data related to this article can be found at http://dx.doi.org/10.1016/j.atmosenv.2017.05.049.

References

Anderson, D.C., Loughner, C.P., Diskin, G., Weinheimer, A., Canty, T.P., Salawitch, R.J., Worden, H.M., Fried, A., Mikoviny, T., Wisthaler, A., Dickerson, R.R., 2014. Measured and modeled CO and NOy in DISCOVER-AQ: an evaluation of emissions and chemistry over the eastern US. Atmos. Environ. 96, 78–87.

Archibald, A.T., Jenkin, M.E., Shallcross, D.E., 2010. An isoprene mechanism intercomparison. Atmos. Environ. 44, 5356–5364.

Atkinson, R., Baulch, D.L., Cox, R.A., Crowley, J.N., Hampson, R.F., Hynes, R.G., Jenkin, M.E., Rossi, M.J., Troe, J., Subcommittee, I., 2006. Evaluated kinetic and photochemical data for atmospheric chemistry: volume II - gas phase reactions of organic species. Atmos. Chem. Phys. 6, 3625–4055.

Bates, K.H., Crounse, J.D., St Clair, J.M., Bennett, N.B., Nguyen, T.B., Seinfeld, J.H., Stoltz, B.M., Wennberg, P.O., 2014. Gas phase production and loss of isoprene epoxydiols. J. Phys. Chem. A 118, 1237–1246.

Canty, T.P., Hembeck, L., Vinciguerra, T.P., Anderson, D.C., Goldberg, D.L., Carpenter, S.F., Allen, D.J., Loughner, C.P., Salawitch, R.J., Dickerson, R.R., 2015. Ozone and NOx chemistry in the eastern US: evaluation of CMAQ/CB05 with satellite (OMI) data. Atmos. Chem. Phys. 15, 10965–10982.

Castellanos, P., Marufu, L.T., Doddridge, B.G., Taubman, B.F., Schwab, J.J., Hains, J.C., Ehrman, S.H., Dickerson, R.R., 2011. Ozone, oxides of nitrogen, and carbon monoxide during pollution events over the eastern United States: an evaluation of emissions and vertical mixing. J. Geophys. Res. Atmos. 116.

Cazorla, M., Wolfe, G.M., Bailey, S.A., Swanson, A.K., Arkinson, H.L., Hanisco, T.F., 2015. A new airborne laser-induced fluorescence instrument for *in situ* detection of formaldehyde throughout the troposphere and lower stratosphere. Atmos. Meas. Tech. 8, 541–552.

Coates, J., Butler, T.M., 2015. A comparison of chemical mechanisms using tagged ozone production potential (TOPP) analysis. Atmos. Chem. Phys. 15, 8795–8808.

Crounse, J.D., Paulot, F., Kjaergaard, H.G., Wennberg, P.O., 2011. Peroxy radical isomerization in the oxidation of isoprene. Phys. Chem. Chem. Phys. 13, 13607–13613.

Da Silva, G., Graham, C., Wang, Z.-F., 2010. Unimolecular β-hydroxyperoxy radical decomposition with OH recycling in the photochemical oxidation of isoprene. Environ. Sci. Technol. 44, 250–256.

Donner, L.J., Wyman, B.L., Hemler, R.S., Horowitz, L.W., Ming, Y., Zhao, M., Golaz, J.-C., Ginoux, P., Lin, S.-J., Schwarzkopf, M.D., Austin, J., Alaka, G., Cooke, W.F., Delworth, T.L., Freidenreich, S.M., Gordon, C.T., Griffies, S.M., Held, I.M., Hurlin, W.J., Klein, S.A., Knutson, T.R., Langenhorst, A.R., Lee, H.-C., Lin, Y., Magi, B.I., Malyshev, S.L., Milly, P.C.D., Naik, V., Nath, M.J., Pincus, R., Ploshay, J.J., Ramaswamy, V., Seman, C.J., Shevliakova, E., Sirutis, J.J., Stern, W.F., Stouffer, R.J., Wilson, R.J., Winton, M., Wittenberg, A.T., Zeng, F., 2011. The dynamical core, physical parameterizations, and basic simulation characteristics of the atmospheric component AM3 of the GFDL global coupled model CM3. J. Clim. 24, 3484–3519.

Emery, C., Jung, J., Bonyoung, K., Yarwood, G., 2015. Improvements to CAMx Snow Cover Treatments and Carbon Bond Chemical Mechanism for Winter Ozone. Utah Department of Environmental Quality.

Emmerson, K.M., Evans, M.J., 2009. Comparison of tropospheric gas-phase chemistry schemes for use within global models. Atmos. Chem. Phys. 9, 1831–1845.

Environ, 2016. User's Guide: Comprehensive Air Quality Model with Extensions Version 6.40. Ramboll Environ, Novato, CA.

EPA, 2009. Integrated Science Assessment for Particulate Matter. United States Environmental Protection Agency, Washington, DC.

EPA, 2013. Integrated Science Assessment of Ozone and Related Photochemical Oxidants. United States Environmental Protection Agency, Washington, DC.

Fan, J., Zhang, R., 2004. Atmospheric oxidation mechanism of isoprene. Environ. Chem. 1, 140.

Fiore, A., Jacob, D.J., Liu, H., Yantosca, R.M., Fairlie, T.D., Li, Q., 2003. Variability in surface ozone background over the United States: implications for air quality policy. J. Geophys. Res. Atmos. 108.

Fisher, J.A., Jacob, D.J., Travis, K.R., Kim, P.S., Marais, E.A., Chan Miller, C., Yu, K., Zhu, L., Yantosca, R.M., Sulprizio, M.P., Mao, J., Wennberg, P.O., Crounse, J.D., Teng, A.P., Nguyen, T.B., St Clair, J.M., Cohen, R.C., Romer, P., Nault, B.A., Wooldridge, P.J., Jimenez, J.L., Campuzano-Jost, P., Day, D.A., Hu, W., Shepson, P.B., Xiong, F., Blake, D.R., Goldstein, A.H., Misztal, P.K., Hanisco, T.F., Wolfe, G.M., Ryerson, T.B., Wisthaler, A., Mikoviny, T., 2016. Organic nitrate chemistry and its implications for nitrogen budgets in an isoprene- and monoterpene-rich atmosphere: constraints from aircraft (SEAC4RS) and ground-based (SOAS) observations in the Southeast US. Atmos. Chem. Phys. 16, 5969–5991.

Fujita, E.M., Campbell, D.E., Zielinska, B., Chow, J.C., Lindhjem, C.E., DenBleyker, A., Bishop, G.A., Schuchmann, B.G., Stedman, D.H., Lawson, D.R., 2012. Comparison of the MOVES2010a, MOBILE6.2, and EMFAC2007 mobile source emission models with on-road traffic tunnel and remote sensing measurements. J. Air Waste Manage 62, 1134–1149.

Goldberg, D.L., Vinciguerra, T.P., Anderson, D.C., Hembeck, L., Canty, T.P., Ehrman, S.H., Martins, D.K., Stauffer, R.M., Thompson, A.M., Salawitch, R.J., Dickerson, R.R., 2016. CAMx ozone source attribution in the eastern United States using guidance from observations during DISCOVER-AQ Maryland. Geophys. Res. Lett. 43, 2249–2258.

Guenther, A.B., Jiang, X., Heald, C.L., Sakulyanontvittaya, T., Duhl, T., Emmons, L.K., Wang, X., 2012. The Model of Emissions of Gases and Aerosols from Nature version 2.1 (MEGAN2.1): an extended and updated framework for modeling biogenic emissions. Geosci. Model Dev. 5, 1471–1492.

Hildebrandt Ruiz, L., Yarwood, G., 2013. Interactions between organic aerosol and NOy: Influence on oxidant production. Texas Air Quality Research Program.

IPCC, 2013. Climate change 2013: the physical science basis. Contribution of Working Group I to the Fifth Assessment Report of the Intergovernmental Panel on Climate Change. Cambridge University Press, Cambridge, United Kingdom and New York, NY, USA.

Jacobs, M.I., Burke, W.J., Elrod, M.J., 2014. Kinetics of the reactions of isoprene-derived hydroxynitrates: gas phase epoxide formation and solution phase hydrolysis. Atmos. Chem. Phys. 14, 8933–8946.

Jenkin, M.E., Young, J.C., Rickard, A.R., 2015. The MCM v3.3.1 degradation scheme for isoprene. Atmos. Chem. Phys. 15, 11433–11459.

Kim, P.S., Jacob, D.J., Fisher, J.A., Travis, K., Yu, K., Zhu, L., Yantosca, R.M., Sulprizio, M.P., Jimenez, J.L., Campuzano-Jost, P., Froyd, K.D., Liao, J., Hair, J.W., Fenn, M.A., Butler, C.F., Wagner, N.L., Gordon, T.D., Welti, A., Wennberg, P.O., Crounse, J.D., St Clair, J.M., Teng, A.P., Millet, D.B., Schwarz, J.P., Markovic, M.Z., Perring, A.E., 2015. Sources, seasonality, and trends of southeast US aerosol: an integrated analysis of surface, aircraft, and satellite observations with the GEOS-Chem chemical transport model. Atmos. Chem. Phys. 15, 10411–10433.

Knote, C., Tuccella, P., Curci, G., Emmons, L.K., Orlando, J.J., Madronich, S., Baró, R., Jiménez-Guerrero, P., Luecken, D.J., Hogrefe, C., Forkel, R., Werhahn, J., Hirtl, M., Pérez, J.L., San José, R., Giordano, L., Brunner, D., Yahya, K., Zhang, Y., 2015. Influence of the choice of gas-phase mechanism on predictions of key gaseous pollutants during the AQMEII phase-2 intercomparison. Atmos. Environ. 115, 553–568.

Kroll, J.H., Ng, N.L., Murphy, S.M., Flagan, R.C., Seinfeld, J.H., 2006. Secondary organic aerosol formation from isoprene photooxidation. Environ. Sci. Technol. 40, 1869–1877.

Lerner, B.M., Gilman, J.B., Aikin, K.C., Atlas, E.L., Goldan, P.D., Graus, M., Hendershot, R., Isaacman-VanWertz, G.A., Koss, A., Kuster, W.C., Lueb, R.A., McLaughlin, R.J., Peischl, J., Sueper, D., Ryerson, T.B., Tokarek, T.W., Warneke, C., Yuan, B., de Gouw, J.A., 2017. An improved, automated whole air sampler and gas chromatography mass spectrometry analysis system for volatile organic compounds in the atmosphere. Atmos. Meas. Tech. 10, 291–313.

Lin, Y.-H., Zhang, H., Pye, H.O.T., Zhang, Z., Marth, W.J., Park, S., Arashiro, M., Cui, T., Budisulistiorini, S.H., Sexton, K.G., Vizuete, W., Xie, Y., Luecken, D.J., Piletic, I.R., Edney, E.O., Bartolotti, L.J., Gold, A., Surratt, J.D., 2013. Epoxide as a precursor to secondary organic aerosol formation from isoprene photooxidation in the presence of nitrogen oxides. P. Natl. Acad. Sci. U. S. A. 110, 6718–6723.

Mao, J., Horowitz, L.W., Naik, V., Fan, S., Liu, J., Fiore, A.M., 2013a. Sensitivity of tropospheric oxidants to biomass burning emissions: implications for radiative forcing. Geophys. Res. Lett. 40, 1241–1246.

Mao, J., Paulot, F., Jacob, D.J., Cohen, R.C., Crounse, J.D., Wennberg, P.O., Keller, C.A., Hudman, R.C., Barkley, M.P., Horowitz, L.W., 2013b. Ozone and organic nitrates over the eastern United States: sensitivity to isoprene chemistry. J. Geophys. Res. Atmos. 118, 11256–11268.

Marais, E.A., Jacob, D.J., Jimenez, J.L., Campuzano-Jost, P., Day, D.A., Hu, W., Krechmer, J., Zhu, L., Kim, P.S., Miller, C.C., Fisher, J.A., Travis, K., Yu, K., Hanisco, T.F., Wolfe, G.M., Arkinson, H.L., Pye, H.O.T., Froyd, K.D., Liao, J., McNeill, V.F., 2016. Aqueous-phase mechanism for secondary organic aerosol formation from isoprene: application to the southeast United States and co-benefit of SO2 emission controls. Atmos. Chem. Phys. 16, 1603–1618.

Marais, E.A., Jacob, D.J., Kurosu, T.P., Chance, K., Murphy, J.G., Reeves, C., Mills, G., Casadio, S., Millet, D.B., Barkley, M.P., Paulot, F., Mao, J., 2012. Isoprene emissions in Africa inferred from OMI observations of formaldehyde columns. Atmos. Chem. Phys. 12, 6219–6235.

Meller, R., Moortgat, G.K., 2000. Temperature dependence of the absorption cross sections of formaldehyde between 223 and 323 K in the wavelength range 225–375 nm. J. Geophys. Res. Atmos. 105, 7089–7101.

Millet, D.B., Jacob, D.J., Boersma, K.F., Fu, T.-M., Kurosu, T.P., Chance, K., Heald, C.L., Guenther, A.B., 2008. Spatial distribution of isoprene emissions from North America derived from formaldehyde column measurements by the OMI satellite sensor. J. Geophys. Res. Atmos. 113.

Naik, V., Horowitz, L.W., Fiore, A.M., Ginoux, P., Mao, J., Aghedo, A.M., Levy, H., 2013. Impact of preindustrial to present-day changes in short-lived pollutant emissions on atmospheric composition and climate forcing. J. Geophys. Res. Atmos. 118, 8086–8110.

Novelli, P.C., Lang, P.M., Masarie, K.A., Hurst, D.F., Myers, R., Elkins, J.W., 1999. Molecular hydrogen in the troposphere: global distribution and budget. J. Geophys.

Res. Atmos. 104, 30427–30444.
Palmer, P.I., Jacob, D.J., Fiore, A.M., Martin, R.V., Chance, K., Kurosu, T.P., 2003. Mapping isoprene emissions over North America using formaldehyde column observations from space. J. Geophys. Res. Atmos. 108.
Park, J., Jongsma, C.G., Zhang, R., North, S.W., 2003. Cyclization reactions in isoprene derived β-hydroxy radicals: implications for the atmospheric oxidation mechanism. Phys. Chem. Chem. Phys. 5, 3638–3642.
Paulot, F., Crounse, J.D., Kjaergaard, H.G., Kroll, J.H., Seinfeld, J.H., Wennberg, P.O., 2009a. Isoprene photooxidation: new insights into the production of acids and organic nitrates. Atmos. Chem. Phys. 9, 1479–1501.
Paulot, F., Crounse, J.D., Kjaergaard, H.G., Kurten, A., St Clair, J.M., Seinfeld, J.H., Wennberg, P.O., 2009b. Unexpected epoxide formation in the gas-phase photooxidation of isoprene. Science 325, 730–733.
Paulson, S.E., Seinfeld, J.H., 1992. Development and evaluation of a photooxidation mechanism for isoprene. J. Geophys. Res. Atmos. 97, 20703–20715.
Peeters, J., Müller, J.F., 2010. HOx radical regeneration in isoprene oxidation via peroxy radical isomerisations. II: experimental evidence and global impact. Phys. Chem. Chem. Phys. 12, 14227–14235.
Peeters, J., Muller, J.F., Stavrakou, T., Nguyen, V.S., 2014. Hydroxyl radical recycling in isoprene oxidation driven by hydrogen bonding and hydrogen tunneling: the upgraded LIM1 mechanism. J. Phys. Chem. A 118, 8625–8643.
Peeters, J., Nguyen, T.L., Vereecken, L., 2009. HOx radical regeneration in the oxidation of isoprene. Phys. Chem. Chem. Phys. 11, 5935–5939.
Pöschl, U., von Kuhlmann, R., Poisson, N., Crutzen, P.J., 2000. Development and intercomparison of condensed isoprene oxidation mechanisms for global atmospheric modeling. J. Atmos. Chem. 37, 29–52.
Reidmiller, D.R., Fiore, A.M., Jaffe, D.A., Bergmann, D., Cuvelier, C., Dentener, F.J., Duncan, B.N., Folberth, G., Gauss, M., Gong, S., Hess, P., Jonson, J.E., Keating, T., Lupu, A., Marmer, E., Park, R., Schultz, M.G., Shindell, D.T., Szopa, S., Vivanco, M.G., Wild, O., Zuber, A., 2009. The influence of foreign vs. North American emissions on surface ozone in the US. Atmos. Chem. Phys. 9, 5027–5042.
Rivera-Rios, J.C., Nguyen, T.B., Crounse, J.D., Jud, W., St Clair, J.M., Mikoviny, T., Gilman, J.B., Lerner, B.M., Kaiser, J.B., de Gouw, J., Wisthaler, A., Hansel, A., Wennberg, P.O., Seinfeld, J.H., Keutsch, F.N., 2014. Conversion of hydroperoxides to carbonyls in field and laboratory instrumentation: observational bias in diagnosing pristine versus anthropogenically controlled atmospheric chemistry. Geophys. Res. Lett. 41, 8645–8651.
Saunders, S.M., Jenkin, M.E., Derwent, R.G., Pilling, M.J., 2003. Protocol for the development of the Master Chemical Mechanism, MCM v3 (Part A): tropospheric degradation of non-aromatic volatile organic compounds. Atmos. Chem. Phys. 3, 161–180.
Saylor, R.D., Stein, A.F., 2012. Identifying the causes of differences in ozone production from the CB05 and CBMIV chemical mechanisms. Geosci. Model Dev. 5, 257–268.
Sherwen, T., Schmidt, J.A., Evans, M.J., Carpenter, L.J., Großmann, K., Eastham, S.D., Jacob, D.J., Dix, B., Koenig, T.K., Sinreich, R., Ortega, I., Volkamer, R., Saiz-Lopez, A., Prados-Roman, C., Mahajan, A.S., Ordóñez, C., 2016. Global impacts of tropospheric halogens (Cl, Br, I) on oxidants and composition in GEOS-Chem. Atmos. Chem. Phys. 16, 12239–12271.
Sillman, S., 1995. The use of NOy, H2O2, and HNO3 as indicators for ozone-NOx-hydrocarbon sensitivity in urban locations. J. Geophys. Res. Atmos. 100, 14175–14188.
Squire, O.J., Archibald, A.T., Griffiths, P.T., Jenkin, M.E., Smith, D., Pyle, J.A., 2015. Influence of isoprene chemical mechanism on modelled changes in tropospheric ozone due to climate and land use over the 21st century. Atmos. Chem. Phys. 15, 5123–5143.
St Clair, J.M., Rivera-Rios, J.C., Crounse, J.D., Praske, E., Kim, M.J., Wolfe, G.M., Keutsch, F.N., Wennberg, P.O., Hanisco, T.F., 2016. Investigation of a potential HCHO measurement artifact from ISOPOOH. Atmos. Meas. Tech. 9, 4561–4568.
Surratt, J.D., Chan, A.W.H., Eddingsaas, N.C., Chan, M., Loza, C.L., Kwan, A.J., Hersey, S.P., Flagan, R.C., Wennberg, P.O., Seinfeld, J.H., 2010. Reactive intermediates revealed in secondary organic aerosol formation from isoprene. P. Natl. Acad. Sci. U. S. A. 107, 6640–6645.
Surratt, J.D., Murphy, S.M., Kroll, J.H., Ng, N.L., Hildebrandt, L., Sorooshian, A., Szmigielski, R., Vermeylen, R., Maenhaut, W., Claeys, M., Flagan, R.C., Seinfeld, J.H., 2006. Chemical composition of secondary organic aerosol formed from the photooxidation of isoprene. J. Phys. Chem. A 110, 9665–9690.
Teng, A.P., Crounse, J.D., Wennberg, P.O., 2017. Isoprene peroxy radical dynamics. J. Am. Chem. Soc. 139, 5367–5377.
Trainer, M., Williams, E.J., Parrish, D.D., Buhr, M.P., Allwine, E.J., Westberg, H.H., Fehsenfeld, F.C., Liu, S.C., 1987. Models and observations of the impact of natural hydrocarbons on rural ozone. Nature 329, 705–707.
Travis, K.R., Jacob, D.J., Fisher, J.A., Kim, P.S., Marais, E.A., Zhu, L., Yu, K., Miller, C.C., Yantosca, R.M., Sulprizio, M.P., Thompson, A.M., Wennberg, P.O., Crounse, J.D., St Clair, J.M., Cohen, R.C., Laughner, J.L., Dibb, J.E., Hall, S.R., Ullmann, K., Wolfe, G.M., Pollack, I.B., Peischl, J., Neuman, J.A., Zhou, X., 2016. Why do models overestimate surface ozone in the Southeast United States? Atmos. Chem. Phys. 16, 13561–13577.
Tuazon, E.C., Atkinson, R., 1990. A product study of the gas-phase reaction of isoprene with the OH radical in the presence of NOx. nt. J. Chem. Kinet. 22, 1221–1236.
von Kuhlmann, R., Lawrence, M.G., Pöschl, U., Crutzen, P.J., 2004. Sensitivities in global scale modeling of isoprene. Atmos. Chem. Phys. 4, 1–17.
Warneke, C., Trainer, M., de Gouw, J.A., Parrish, D.D., Fahey, D.W., Ravishankara, A.R., Middlebrook, A.M., Brock, C.A., Roberts, J.M., Brown, S.S., Neuman, J.A., Lerner, B.M., Lack, D., Law, D., Hübler, G., Pollack, I., Sjostedt, S., Ryerson, T.B., Gilman, J.B., Liao, J., Holloway, J., Peischl, J., Nowak, J.B., Aikin, K.C., Min, K.E., Washenfelder, R.A., Graus, M.G., Richardson, M., Markovic, M.Z., Wagner, N.L., Welti, A., Veres, P.R., Edwards, P., Schwarz, J.P., Gordon, T., Dube, W.P., McKeen, S.A., Brioude, J., Ahmadov, R., Bougiatioti, A., Lin, J.J., Nenes, A., Wolfe, G.M., Hanisco, T.F., Lee, B.H., Lopez-Hilfiker, F.D., Thornton, J.A., Keutsch, F.N., Kaiser, J., Mao, J., Hatch, C.D., 2016. Instrumentation and measurement strategy for the NOAA SENEX aircraft campaign as part of the Southeast Atmosphere Study 2013. Atmos. Meas. Tech. 9, 3063–3093.
Wolfe, G.M., Crounse, J.D., Parrish, J.D., St Clair, J.M., Beaver, M.R., Paulot, F., Yoon, T.P., Wennberg, P.O., Keutsch, F.N., 2012. Photolysis, OH reactivity and ozone reactivity of a proxy for isoprene-derived hydroperoxyenals (HPALDs). Phys. Chem. Chem. Phys. 14, 7276–7286.
Wolfe, G.M., Kaiser, J., Hanisco, T.F., Keutsch, F.N., de Gouw, J.A., Gilman, J.B., Graus, M., Hatch, C.D., Holloway, J., Horowitz, L.W., Lee, B.H., Lerner, B.M., Lopez-Hilifiker, F., Mao, J., Marvin, M.R., Peischl, J., Pollack, I.B., Roberts, J.M., Ryerson, T.B., Thornton, J.A., Veres, P.R., Warneke, C., 2016a. Formaldehyde production from isoprene oxidation across NOx regimes. Atmos. Chem. Phys. 16, 2597–2610.
Wolfe, G.M., Marvin, M.R., Roberts, S.J., Travis, K.R., Liao, J., 2016b. The framework for 0-d atmospheric modeling (F0AM) v3.1. Geosci. Model Dev. 9, 3309–3319.
Yarwood, G., Rao, S., Yocke, M., Whitten, G.Z., 2005. Updates to the Carbon Bond Chemical Mechanism: CB05. United States Environmental Protection Agency.
Yu, S., Mathur, R., Sarwar, G., Kang, D., Tong, D., Pouliot, G., Pleim, J., 2010. Eta-CMAQ air quality forecasts for O3 and related species using three different photochemical mechanisms (CB4, CB05, SAPRC-99): comparisons with measurements during the 2004 ICARTT study. Atmos. Chem. Phys. 10, 3001–3025.
Zhang, H., Rattanavaraha, W., Zhou, Y., Bapat, J., Rosen, E.P., Sexton, K.G., Kamens, R.M., 2011. A new gas-phase condensed mechanism of isoprene-NOx photooxidation. Atmos. Environ. 45, 4507–4521.
Zhu, L., Jacob, D.J., Kim, P.S., Fisher, J.A., Yu, K., Travis, K.R., Mickley, L.J., Yantosca, R.M., Sulprizio, M.P., De Smedt, I., González Abad, G., Chance, K., Li, C., Ferrare, R., Fried, A., Hair, J.W., Hanisco, T.F., Richter, D., Jo Scarino, A., Walega, J., Weibring, P., Wolfe, G.M., 2016. Observing atmospheric formaldehyde (HCHO) from space: validation and intercomparison of six retrievals from four satellites (OMI, GOME2A, GOME2B, OMPS) with SEAC4RS aircraft observations over the southeast US. Atmos. Chem. Phys. 16, 13477–13490.